

## Electrodeposition of Co-W Alloys with P and Ni

Henrikas CESIULIS<sup>1\*</sup>, Xiaogang XIE<sup>2</sup>, Elizabeth PODLAHA-MURPHY<sup>3</sup>

<sup>1</sup>Department of Physical Chemistry, Vilnius University, Vilnius, Lithuania. Naugarduko 24, LT-03225, Vilnius, Lithuania

<sup>2</sup>Department of Geology and Geophysics, Louisiana State University, E-235 Howe-Russell, Baton Rouge, LA 70803, USA

<sup>3</sup>Department of Chemical Engineering, Northeastern University, Boston, MA 02115, USA

Received 30 October 2008; accepted 23 May 2009

The aim of the present study is to explore the electrolyte composition in order to obtain Co-W, Co-Ni-W, Co-P-W, Co-Ni-P-W alloys with smooth morphology, high reaction rate, and underscoring the interactive reduction behavior of the codepositing elements. The recommended electrolyte formulation: 0.2 M MeSO<sub>4</sub>, 0.4 M Na<sub>2</sub>WO<sub>4</sub>, 0.5 M citric acid, and 1.5 M ammonia (“Me” represents the iron group metal); provides an optimal pH buffer capacity in the range of 7.5 to 8.5 at 70 °C. Smooth and crack free films of Co-W, Co-P-W, Co-Ni-W, and Co-Ni-P-W alloys were electrodeposited. Nanowires and nanotubes of the alloys were realized in alumina templates with constant potential and pulsed potential, respectively. The amount of W in the alloys, deposited on a rotating cylinder electrode galvanostatically, decreased with an increase in P incorporation (from 30 at.% to 15 at.% in alloys Co-P-W, and up to 30 at.% to 1.3 at.% in Co-Ni-P-W at the content of P up to 11 at.%) and also with the amount of Ni (from 30 at.% to 14 at.% in Co-Ni-W). The partial current densities were determined from WDS chemical analyses and weight of the deposits. The Co partial current density was reduced when codeposited with W, and the W partial current density was reduced when P was incorporated into the deposit. The ratio of Ni to Co in the deposited ternary alloys differs from that of the electrolytes, characteristic of the anomalous co-deposition behavior. The anomalous co-deposition of Co with Ni is eliminated when phosphorous is incorporated into the alloys. These interacting reduction observations can be explained by a competing adsorption mechanism. The described baths can be used both for thin film and nanostructures electrodeposition.

**Keywords:** tungsten alloys, phosphorous alloys, electrodeposition, nanowires, nanotubes.

### 1. INTRODUCTION

The interest in electrodeposited tungsten-rich binary and ternary alloys with iron-group metals has increased in recent years due to their unique combination of tribological, magnetic, electrical and electro-erosion properties. Their applications well documented and examples can be found in corrosion protection [1–2], electronics for barrier layers [3], and catalysis [4–5]. Introduction of a third element into binary tungsten alloys in some cases can improve corrosion properties, for example Ni-W-Co alloy had better corrosion resistance than similarly electrodeposited Co-W amorphous alloys [6]. Additionally, low-cost and efficient electrocatalysts are important for fuel cell electrodes and tungsten alloys can be a possible alternative to expensive platinum and alloys containing platinum group metals used today [5]. Electrodeposited tungsten alloys may also find a niche as structures for LIGA applications, a German acronym describing a micro-scale fabrication process: lithography (L) to create a micro-patterned device template, electrodeposition (G) to fill the pattern followed by removal of the template to create a device master, and molding (A) to replicate it, via injection molding, reaction injection molding, hot-embossing, slip casting or extrusion [7–9]. The electroplated microstructures can also be used as the final product in a microelectromechanical system (MEMS). From this point of view, electrodeposited tungsten alloys are useful because of their excellent mechanical properties regarding wear and mechanical durability [7, 10–11], premium hardness [12–14], nanocrystalline structure and smooth

surface [15–18], and throwing power in the case of tungsten alloys electrodeposition in deep recesses [19]. Electrodeposition of NiW alloys in a deep recess for LIGA applications has been demonstrated [9, 10, 19]. Pulsed deposition was key in order to form a deposit with a uniform composition gradient along the growth direction [10, 19].

Electrodeposition in general is an inexpensive route for fabricating nanostructured materials such as nanowires, and nanotubes. Magnetic nanowire/nanorod arrays are considered very promising for application in ultrahigh density magnetic storage devices and nanosensors [20]. Because of the high degree of ordering and thermal and chemical stability of nanoporous alumina membranes these have been widely used as templates for electrodeposited nanowires and tubes [21–29]. Outside of the work presented here there are no reports of electrodeposited tungsten alloy nanowires or nanotubes.

Moreover, in order to fill up nanosized pores entirely as much as possible, the grain size of electrodepositing metal or alloy should be small, i. e. electrodeposits have to be nanocrystalline. If the electroforming of MEMS or similar microdevices is of concern, the obtained electrodeposits also should be crack free and their surface should have low roughness. To achieve these requirements electrodeposition of ternary tungsten-rich alloys instead of the binary alloys, can alter the structure, for example Ni-Fe-W instead of Ni-W [16] reduced the amount of cracks, or adding phosphorous to electrodeposited alloys [30–32], induces a small grain size. Therefore, the aim of the present study is to design an electrolyte and the associated operating conditions to obtain crack free, magnetic alloy electrodeposits rich in tungsten: Co-W, Co-Ni-W, Co-P-

\*Corresponding author. Tel.: +370-5-2193183; fax.: +370-5-233 0987.  
E-mail address: henrikas.cesiulis@chf.vu.lt (H. Cesiulis)

W, Co-Ni-P-W and to explore the electrodeposition of the tungsten alloy nanowires and nanotubes in aluminum oxide templates.

## 2. EXPERIMENTAL PROCEDURE

Tungsten alloys films were deposited on a rotating cylinder electrode (RCE) using Autolab HT RotaHull equipment for current and rotation control. Mechanically polished copper cylinders ( $\varnothing$  5 mm and working area 15 cm<sup>2</sup>) were used as a working electrode. Before electrodeposition the cylinders were chemically-mechanically polished by a commercially available polishing emulsion, CuproNet, rinsed in distilled water, followed by a 10 % sulfuric acid rinse for removal of any oxides, and then degreased by distilled water and acetone. A platinum plated titanium mesh was used as the counter electrode. The electrodeposition was carried out at 200 rpm, and temperature was kept at 70 °C. Qualitative elemental analysis of the obtained alloys was carried out by energy-dispersive X-ray spectroscopy (EDS).

The buffer capacity of the plating bath solution was determined by titration with 15 M NaOH solution to avoid any dilution effects. Changes in pH were monitored with pH-meter ThermoOrion, type 420. CurveExpert software (D. Hyams) was used for the digital differentiation of the titration curves and extraction of the buffer capacity, which is defined as  $\frac{\partial n}{\partial \text{pH}}$ , where  $n$  is the change in concentration of a base or acid over the change of pH.

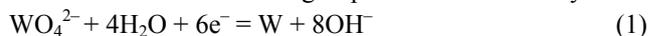
Commercially available anodized aluminum oxide (AAO), Whatman Anodiscs nanoporous membranes were used as templates for electrodeposition of nanowires and nanotubes. The manufacturer-specified pore diameter and length were 200 nm and 60 nm, respectively. For the electrical contact Au was sputtered on one side of template. The Au-coated template acted as the working electrode and was fixed inside a stationary polymeric (PEEK) holder. The cathode membrane was positioned horizontally opposing a platinum counter electrode. After the alloys were deposited, part of the obtained sample was dissolved in 1 M NaOH for scanning electron microscopy (SEM). SEM analysis was carried out with a JEOL JSM-840A.

## 3. RESULTS AND DISCUSSIONS

**Buffer capacity examination.** Tungsten alloys with iron group metals are typically electrodeposited from citrate ammonia electrolytes with tungstate ions and iron-group metal sulfates namely  $\text{MeSO}_4 + \text{Na}_2\text{WO}_4 + \text{Na}_3\text{Cit} + \text{NH}_3$  (where “Me” represents the iron group metal). There are two principal solutions reported in the literature for electrolytes containing a small amount of Me(II), 0.02 M [12, 16], and a higher amount of Me(II) 0.2 M [11, 19]. The use of the more concentrated electrolyte has resulted in little to no variation in the deposit composition over a wide range of current densities. This may be a consequence of ensuring a kinetic control of the deposition process. Thus, the electrolyte concentration of 0.2 M of the iron group metal(s) has been selected here.

Electrodeposition of tungsten alloys from aqueous baths generally is carried out in non-hermetic cells. In this case, a sufficient part of ammonia can evaporate during

long-term electrodeposition at elevated temperatures that result in a decreasing pH and affect the deposition rate, alloy composition and current efficiency [6, 16–19, 33–35]. Therefore, the pH of the electrolyte has been examined. Moreover, in the case of W- alloy electrodeposition the electroreduction of  $\text{WO}_4^{2-}$ -ion to W is associated with increasing of pH in the reaction layer:



In addition, electrodeposition of W alloys is accompanied by  $\text{H}_2$  evolution:



That yields an alkalization of a pre-electrode layer that can sufficiently decrease the W content in the alloys [34–35]. Therefore, the buffer capacity of the electrolyte should be maximized.

The buffer capacity is shown in Fig. 1, at room temperature. Two peaks are present, one at pH ~7.25 and the other at pH ~10, with the largest peak indicating the highest buffering ability and dependent upon the amount of ammonia in the electrolyte. In the range of pH 6.5–8.5 buffering is low and is controlled mainly by the presence of citrates. After ammonia had been added to the electrolyte the buffering capacity increases dramatically in the region between  $9 < \text{pH} < 11$ . The maximum in the range of pH ~10 depends on the concentration of ammonia. A deep minimum occurs at pH ~8.5 which indicates the electrolyte pH to avoid with the worst buffering capacity.

Since electrodeposition of W alloys is often carrying out at elevated temperatures, the buffer capacities of solutions at 70 °C with higher concentrations of ammonia are presented in Fig. 2. The data is compared to the same ammonia concentrations at 23 °C. When the concentration of ammonia is 0.8 M, the minimum buffer capacity at 70 °C is not as deep as at room temperature. When the concentration of ammonia increases, the minimum of buffer capacity disappears. The maximum in buffer capacity shifts to lower pH values when the electrolyte temperature is increased. For example, near room temperature a pH of 8.5 would not be a good electrolyte choice, but at 70 °C it is a preferred value.

In order to reduce possible evaporation of ammonia from the electrolytes during long-term electrolysis at elevated temperatures and thereby keeping the alloy deposition rate stable and offset the increase in pH values because of the reactions (1) and (2), the electrodeposition was performed at lowest pH as possible. Therefore, most experiments were done at pH 7.5–8.1, i. e. at a pH when a sufficient part of ammonia added in the solutions transforms into the non-volatile  $\text{NH}_4^+$ -ionic form. Moreover, because of better buffering properties of solutions at these pH values, the higher concentration (1.5 M) of ammonia is used for the following investigations: 0.2 M  $\text{CoSO}_4 + 0.5$  M  $\text{Na}_2\text{HCitr} + 0.4$  M  $\text{Na}_2\text{WO}_4 + 1.5$  M  $\text{NH}_3$ .

**Co-W electrodeposition.** The dependency of current density on W content in Co-W alloys at variable pH, at  $t = 70$  °C is presented in Fig. 3. The content of W in Co-W alloys goes through a maximum with pH and is effected by the current density. The highest W content is obtained in the range of pH 7.0–8.1 and can reach 30 at.%, whereas at lower and higher pH the alloys contain a smaller amount of W (max. ~22 at.% of W). In addition, the amount of W

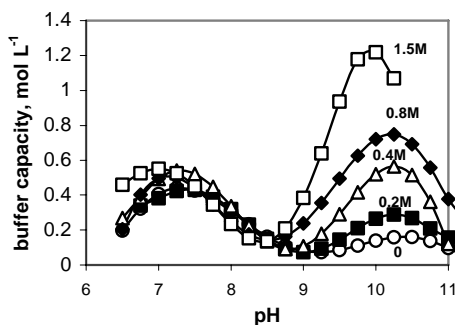


**Fig. 1.** Buffer capacity vs. pH at various ammonia concentrations (23 °C). The concentration of ammonia in solution is indicated next to curves. Formulation of the solution: 0.2 M CoSO<sub>4</sub> + 0.5 M Na<sub>2</sub>HCit + 0.4 M Na<sub>2</sub>WO<sub>4</sub>

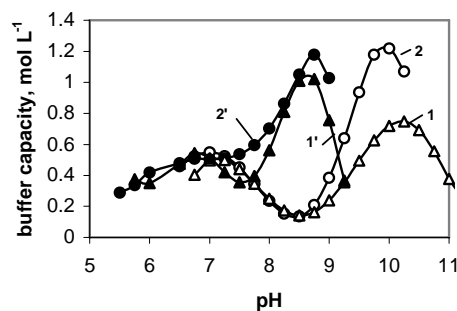


**Fig. 2.** Buffer capacity vs. pH at different temperatures. Formulation of solution: 0.2 M CoSO<sub>4</sub> + 0.5 M Na<sub>2</sub>Hcit + 0.4 M Na<sub>2</sub>WO<sub>4</sub> + x M ammonia. 1 and 1' – for x = 0.8 M; 2 and 2' – for x = 1.5 M. 1 and 2 – at 23 °C; 1' and 2' – at 70 °C

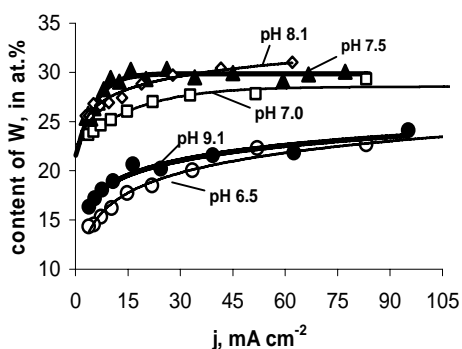


**Fig. 3.** Content of W in Co-W alloys as a function of current density at various pH (indicated next to curves)

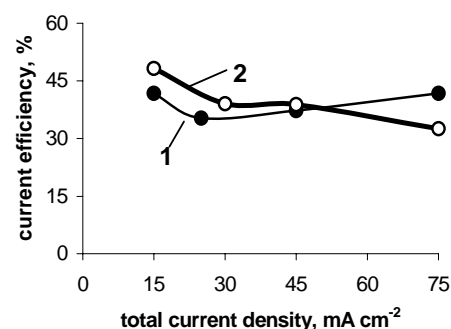


**Fig. 4.** Current efficiencies for elemental Co (1) and Co-W alloys (2) electrodeposition from the solution 0.2 M CoSO<sub>4</sub> + 0.4 M Na<sub>2</sub>WO<sub>4</sub> + 0.5 M citric acid + 1.5 M NH<sub>3</sub> at pH 7.5 and 70 °C

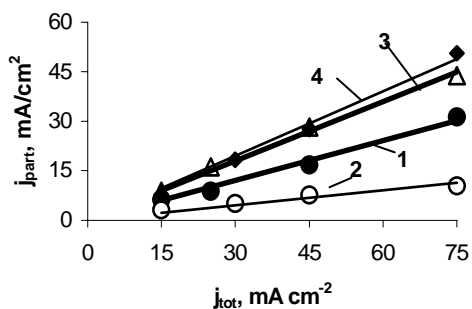
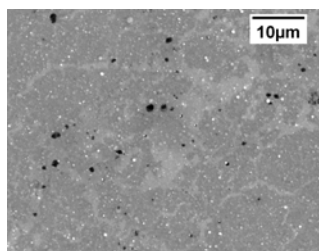
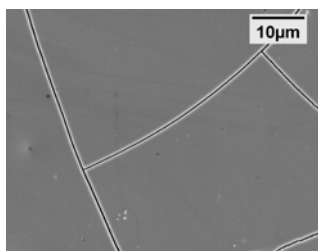


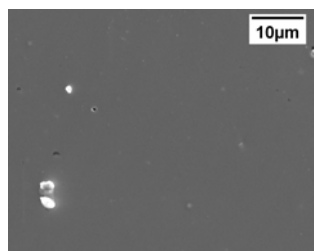
**Fig. 5.** Partial current densities for Co and H<sub>2</sub> during pure Co and Co-W alloy electrodeposition as a function of total current density: 1, 3 – for Co and H<sub>2</sub> during pure Co deposition, respectively; 2, 4 – for Co and H<sub>2</sub> during CoW alloys deposition, respectively. The composition of the bath as indicated in Fig. 4; pH 7.5



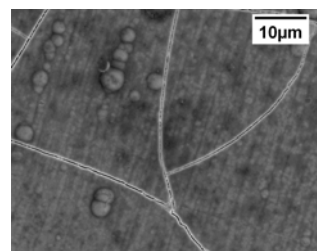
a



b



a



b

**Fig. 6.** SEM images of Co-W alloys electrodeposited at pH 7.5: a – at  $j = 15 \text{ mA/cm}^2$ , b – at  $j = 45 \text{ mA/cm}^2$ . Content of W 30 at.%, thickness of film 12 and 13  $\mu\text{m}$ , respectively

**Fig. 7.** SEM images of Co-W alloys electrodeposited at pH 9.1: a – at  $j = 15 \text{ mA/cm}^2$ , b – at  $j = 45 \text{ mA/cm}^2$ . Content of W 21 at.% and 22 at.%, respectively; thickness of film (10 – 11)  $\mu\text{m}$

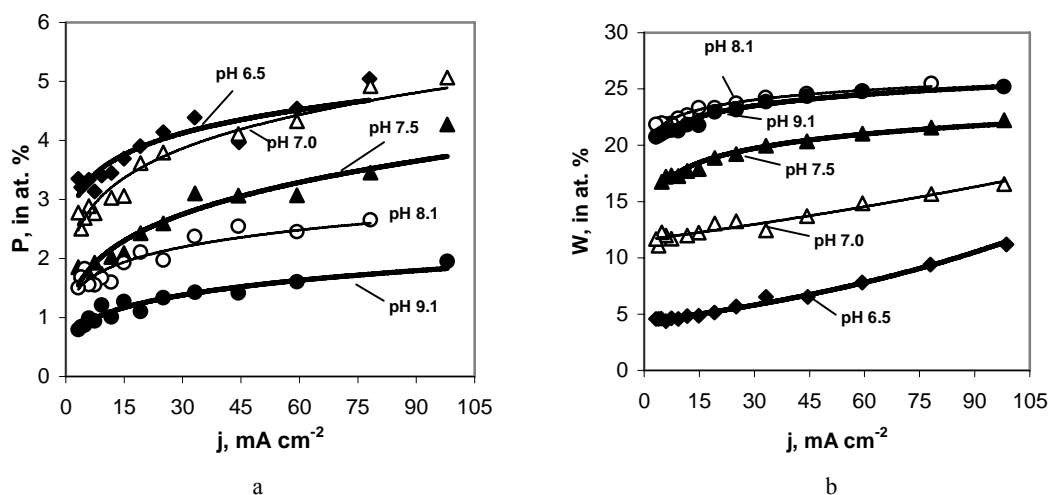


**Fig. 8.** Content of phosphorous (A) and tungsten (B) in the Co-W-P alloys obtained at various pH from the bath: 0.2 M  $\text{CoSO}_4$  + 0.4 M  $\text{Na}_2\text{WO}_4$  + 0.5 M citric acid + 1.5 M ammonia + 0.05M  $\text{NaH}_2\text{PO}_2$ . Values of pH are indicated next to curves

in alloys increases with current density and then becomes insensitive to the effect of current densities at values exceeding  $15 \text{ mA/cm}^2$  for the pH range of 7.0–8.1; at pH 9.1 and 6.5 the W content increased slightly beyond  $15 \text{ mA/cm}^2$ . As a consequence of the high concentration of Co(II) and W(VI) in the bath, the current efficiency is moderately high (see Fig. 4), between 50 %–30 %, where the lowest current efficiency is observed at the highest applied current density, as expected and consistent with other literature reports on W-alloys, such as [33, 36]. Also in Fig. 5 the partial current densities of Co and the side reaction during elemental Co deposition and when it is codeposited as an alloy with W are presented. During the W codeposition, the partial current densities for the side reaction (mainly for  $\text{H}_2$  evolution) remain almost the same as in the case of pure Co electrodeposition. Whereas, the partial current densities for Co significantly decreases in the case of CoW alloy electrodeposition, i. e. W inhibits the reduction of Co(II) that is in accordance with the induced co-deposition model proposed in [10, 37]. Thus, the CE of the alloy is comparable to the elemental deposition of Co; even though the Co partial current density is lowered, the additional W partial current density contributes to the total metal reaction rate and hence efficiency.

Electrodeposited Co-W alloys have an appearance of grey-white and shiny. The SEM images of Co-W alloys electrodeposited from the electrolytes at pH 7.5 and 9.1 are presented in Figs. 6 and 7, respectively. Electrodeposited alloys at low current densities ( $15\text{--}30 \text{ mA/cm}^2$ ) are free of cracks, but cracks formed at higher current densities. On the other hand, nodules formed at low current density at pH 7.5, and at high current density at pH 9.1. At pH 7.5 and  $15 \text{ mA/cm}^2$  small nodules have an average size of approx. 300 nm (see Fig. 6). Whereas electrodeposited alloys at pH 9.1 and  $15 \text{ mA/cm}^2$  are extremely smooth, their roughness is significantly greater at  $45 \text{ mA/cm}^2$  than that observed at any current density at pH 7.5 (see Fig. 7).

**Co-P-W electrodeposition.**  $\text{NaH}_2\text{PO}_2$  usually is used as a source of phosphorous for P-containing electrodepos-

ited alloys. In addition, due to its oxidizing ability, sodium hypophosphite prevents Co(II) oxidation to Co(III) when the bath is exposed to air.

In the presence of  $\text{NaH}_2\text{PO}_2$  the composition of the deposit depends on both solution pH and concentration of  $\text{NaH}_2\text{PO}_2$ . The effect of pH on the P and W contents in the alloys are presented in Fig. 8 A and B. At pH 6.5–7.0 the amount of P in the alloys is similar and then almost linearly decreases when the pH increases. In contrast, the amount of W increases linearly with increasing pH from 6.5 to 8.1 and remains almost the same level at pH 9.1.

Comparing the amount of W in the CoW deposit with (Fig. 8, b) and without (Fig. 3) P shows that the amount of W in the alloys is influenced by the addition of the  $\text{NaH}_2\text{PO}_2$  in the electrolyte. As the amount of phosphorous in the alloys increases, the ratio of W:Co is reduced sufficiently. For example at pH 7.5  $\text{mA cm}^{-2}$  and  $30 \text{ mA cm}^{-2}$  the ratio of W:Co drops from 0.43 (Co-W) to 0.23 (Co-P-W) at the amount of P 3.1 at.%. An even sharper decrease in W amount in Ni-W-P alloys due to the presence of  $\text{NaH}_2\text{PO}_2$  was described with similar concentrations of sodium hypophosphite [38].

The current efficiency for Co-W-P electrodeposition is larger than Co-W codeposition at low current density (e. g.  $15 \text{ mA cm}^{-2}$ ), and slightly lower at higher current densities, and depends most strongly on current density than on the concentration of sodium hypophosphite (Fig. 9). The higher the current density, the lower the current efficiency. This result is also reflected in the polarization curves obtained at the same pH, presented in Fig. 10. The polarization curves for all the electrolytes with  $\text{NaH}_2\text{PO}_2$  have a higher current density than the Co-W curve and they do not significantly change with changes in  $\text{NaH}_2\text{PO}_2$  concentration. Therefore, the current efficiency for Co-W-P electrodeposition remains almost at the same level with  $\text{NaH}_2\text{PO}_2$ .

Introducing  $\text{NaH}_2\text{PO}_2$  changes the partial current densities, particularly the partial currents for W (Fig. 11). Addition of P in the deposit does not change the Co partial current density (within  $\pm 8\%$ ), but decreases the W partial

current density and thus, results in a decreased amount of tungsten in the ternary deposit (see Fig. 8).

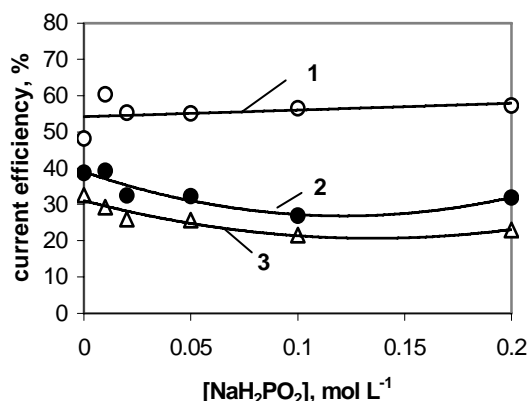


**Fig. 9.** Current efficiency for Co-W-P vs. concentration of sodium hypophosphite at various current densities (pH 7.5). Content of solution – as in Fig. 8: 1 –  $j = 15 \text{ mA/cm}^2$ ; 2 –  $j = 45 \text{ mA/cm}^2$ ; 3 –  $j = 75 \text{ mA/cm}^2$

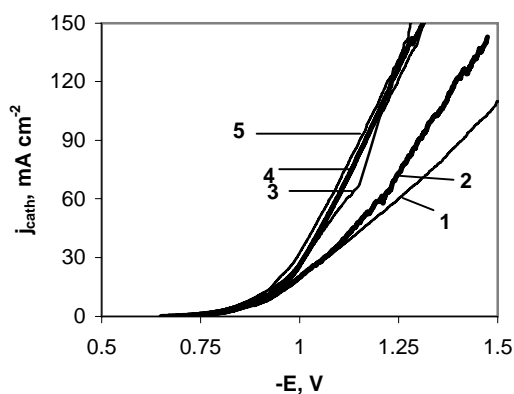
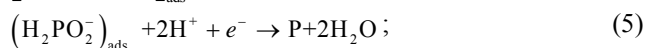
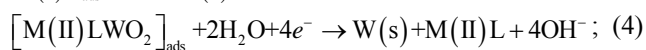


**Fig. 10.** Polarization curves of Co-W electrode at pH 7.5 in the solutions: 1 – 0.4 M Na<sub>2</sub>WO<sub>4</sub> + 0.5 M citric acid + 1.5 M ammonia; 2 – as 1 + 0.2 M CoSO<sub>4</sub>; 3 – as 2 + 0.01 M NaH<sub>2</sub>PO<sub>2</sub>; 4 – as 2 + 0.05 M NaH<sub>2</sub>PO<sub>2</sub>; 5 – as 2 + 0.10 M NaH<sub>2</sub>PO<sub>2</sub>. Potential scan rate 2 mV/s; temperature 70 °C

According to the kinetic models of induced codeposition and reduction of NaH<sub>2</sub>PO<sub>2</sub> [37, 39] both undergo a possible adsorbed intermediate:



where “M” represents the iron group metal, and “s” the solid state.

One explanation for the reduced W content when codeposited with P is that the P-intermediate (5) blocks available sites for the W-intermediate (4), in an analogous idea to the competitive adsorption model presented by Matloz for NiFe codeposition. [40] Partially reduced Co may also form an adsorbed intermediate (3) but the data here suggests that this adsorption step may not be rate controlling for Co, unlike the W and P steps. A more detailed description will be provided in further publications.

Irrespective of the content of P and W the electrodeposited Co-W-P alloys are grey-white and shiny.

Deposits obtained at lower current densities are free of cracks. The nodules that appear in the case of Co-W disappear at concentrations of Na<sub>2</sub>PO<sub>2</sub><sup>-</sup> 0.05 M–0.10 M.

**Adhesion of Co-W and Co-P-W alloys.** The electrodeposited Co-W and Co-W-P, adhered well to the Cu substrate. The deposits obtained on the Cu rod having a diameter of 6 mm can be folded without evident peeling. Only some cracks may appear in the folding area. An example is shown in Fig. 12. It was observed recently [36], that Co-W alloys electrodeposited from citrate baths with boric acid instead of ammonia and with less amount of W (up to 12 at.%), delaminated from Cu substrate due to large internal stress.

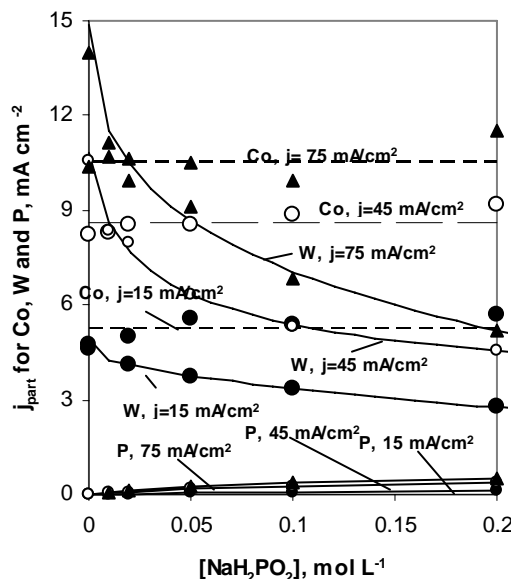


**Fig. 11.** Partial current densities as a function of NaH<sub>2</sub>PO<sub>2</sub> concentration obtained for Co-W-P alloys at certain total current densities and pH 7.5



**Fig. 12.** Optical image of a coated by Co-W (28 at.%) and then folded Ø 6 mm Cu rod. Thickness of deposit ~50 µm, current density 30 mA/cm<sup>2</sup>

**Co-W and Co-P-W with nickel electrodeposition.** The influence of nickel was addressed by varying the ratio  $C_{\text{Ni(II)}}/(C_{\text{Ni(II)}} + C_{\text{Co(II)}})$  in the electrolyte. The composition of the electrolyte was changed in six steps from the pure Co-W (or Co-P-W) bath solution to the pure Ni-W (or Ni-P-W) bath solution keeping the sum of the concentrations Co(II) and Ni(II) constant and equal to 0.2 M. Whereas, concentrations of the remaining components (citrate, ammonia and etc.) were the same as for Co-W alloys electrodeposition as described in the previous sections. The

value of pH was kept at 8.1. For the electrodeposition of P-containing quaternary alloys the electrolytes additionally contained 0.05 M  $\text{NaH}_2\text{PO}_2$ .

The alloy deposit composition dependences of the ternary Co-Ni-W alloy as a function of the ratio Ni(II) to Co(II) in the baths are shown in Fig. 13. The preferential deposition of Ni over that of Co in a wide range of  $C_{\text{Ni(II)}}/(C_{\text{Ni(II)}}+C_{\text{Co(II)}})$  ratios (up to 0.6) takes place, that is characteristic for anomalous codeposition behavior. There is a continuous decrease from the composition value characteristic for Co-W alloy (30 at.% of W) to the value characteristic for Ni-W alloys (<20 at.% of W).

When phosphorous is co-depositing with Co, Ni, and W the alloy content changes with the ratio of  $C_{\text{Ni(II)}}/(C_{\text{Ni(II)}}+C_{\text{Co(II)}})$  in the electrolyte differently from the previous case (see Fig. 14). There is no anomalous codeposition of Ni and Co, their content in the quaternary alloys almost linearly changes with their concentrations in the electrolyte. The content of P in the alloy sufficiently increases (from 2.5 at.% to 11 at.%) with the increasing Ni(II) concentration in the bath. This is the result of the comparatively easier P co-deposition with nickel than with cobalt, and this result was obtained also in other systems [41]. However, introducing phosphorous dramatically reduces the content of W in the quaternary alloys (up to 1 at.% – 5 at.%) especially at the higher ratios of  $C_{\text{Ni(II)}}/(C_{\text{Ni(II)}}+C_{\text{Co(II)}})$  in the electrolytes. In our opinion, the reason for such a reduction is the same as for Co-W-P alloys electrodeposition, preferred adsorption of phosphorous compared to the W-intermediate.

The introduction of phosphorous into W-containing alloys improves the surface morphology as it is shown in Fig. 15. The electrodeposited Ni-W and Co-Ni-W alloys often have cracks, whereas obtained Ni-P-W and Co-Ni-P-W alloys are free of cracks even electrodeposited at higher current densities ( $>30 \text{ mA cm}^{-2}$ ).

**Nanowires and nanotubes electrodeposition in AAO membranes.** A major limiting factor for the adaptability of conventional plating baths to deep recess plating is the variance in hydrodynamic conditions. Namely, despite electrolyte agitation at the mouth of the recess, the electrolyte in the recess remains stagnant creating transport limitations of the reactant species and an undesirable accumulation of unwanted product species. In addition, reactions inherent to the iron-group and W-alloy co-electrodeposition often occur with gas evolving side reactions and hydroxyl ion products that can lead to pH rises and changes in deposit composition. The electrodeposition of Co-W from the buffered electrolytes presented here is adaptable from this point of view, because the content of W is relatively constant over a large pH range (see Fig. 3), and possesses enough buffer capacity (see Figs. 1 and 2). All these features would have to warrant the same alloy composition along the entire length of array.

Two alloy electrolytes were selected, Co-W-P and Co-W, to deposit into AAO nanoporous membranes. For the Co-P-W electrodeposition the solution additionally contained 0.05 M  $\text{NaH}_2\text{PO}_2$ . The electrodeposition was performed under constant potential and pulse potential deposition modes, and the current was monitored to define the end of the wire or tube growth.

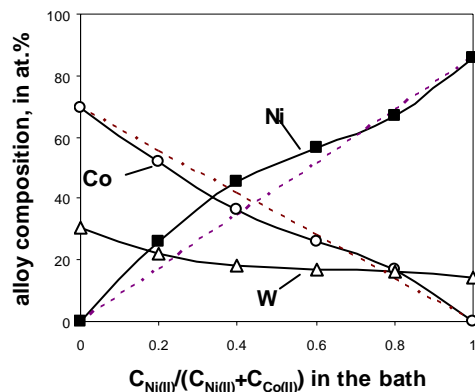


**Fig. 13.** Changes in composition of electrodeposited Co-Ni-W alloys caused by changes in concentrations of Co(II) and Ni(II) in the baths. Current density  $45 \text{ mA cm}^{-2}$ . Dotted lines express the calculated concentrations of Ni and Co in alloys, if the ratio of the concentration in alloy would depend linearly on the ones in the baths

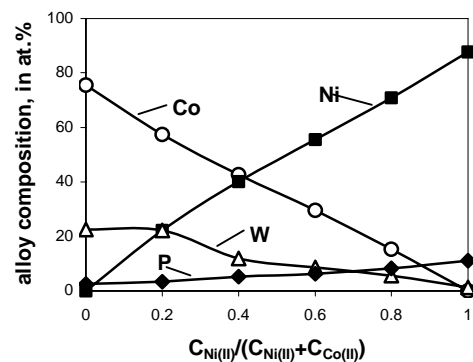


**Fig. 14.** Changes in composition of electrodeposited Co-Ni-W-P alloys caused by changes in concentrations of Co(II) and Ni(II) in the baths. Current density  $45 \text{ mA cm}^{-2}$

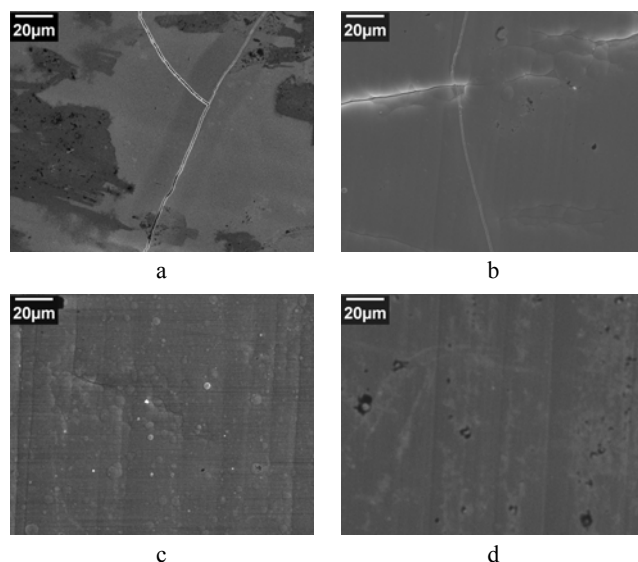


**Fig. 15.** SEM images of ternary and quaternary W-containing alloys obtained at pH 8.1 and current density  $45 \text{ mA cm}^{-2}$ . The thickness of deposits  $10 \mu\text{m} - 12 \mu\text{m}$ . Numbers means element content in alloy (at.%). a – 86Ni-14W; b – 26Co-57Ni-17W; c – 87.3Co-11P-1.3W; d – 29.5Co-55.5Ni-6P-9W

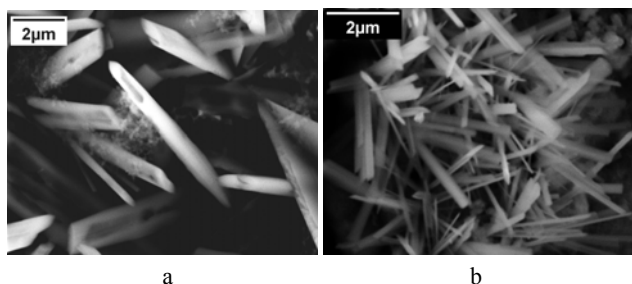


**Fig. 16.** SEM images of the dissolved membrane contained Co-W electrodeposits obtained: a – at constant potential mode, and b – at pulse potential deposition mode. The value of deposition potential amplitude  $E = -1.1$  V

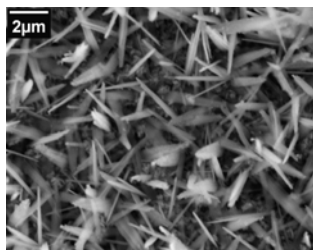


**Fig. 17.** SEM images of the dissolved membrane contained Co-P-W electrodeposits obtained at pulse potential mode. The value of deposition potential amplitude  $E = -1.0$  V

In both modes the amplitude of potential was chosen based on the data presented Fig. 10 corresponding to a potential value that should be attributed to a current density of approx.  $15 \text{ mA cm}^{-2}$  at steady state. At this current density the maximal content of W in the alloys is obtained, as well as the current efficiency is highest because of the reduced evolution of gaseous hydrogen. In pulse potential deposition, the value for a relaxation potential (current equal to zero) was set as  $-0.66$  V. The pulse duration was 10 sec, the relaxation duration was 30 sec, and the total number of cycles was 1500.

The images of the nanostructures after the membrane was dissolved in KOH are presented in Figs. 16 and 17. At the constant potential mode nanotubes were obtained (Fig. 16, a), whereas at pulse potential mode nanowires formed (Fig. 16, b). These differences in the obtained shapes of the nanostructure are probably a consequence of the different conditions for hydrogen evolution from the pores. At the deposition in constant potential mode hydrogen evolves simultaneously with the electrodeposition of alloy in the recess and blocks the central part of the pores shielding deposition from the pore center forming nanotubes. In pulse potential mode the evolved hydrogen and the products associated with hydrogen evolution (increased concentration of  $\text{OH}^-$ ) has time to diffuse out of the pore during the relaxation time and the alloy can fill up the whole volume of the pore, resulting in nanowires.

#### 4. CONCLUSIONS

1. A common electrolyte with the best observed buffer capacity for the various electrodeposited W-containing binary, ternary and quaternary alloys, Co-W, Ni-W, Co-P-W, Co-Ni-W, and Co-Ni-P-W is  $0.2 \text{ M MeSO}_4 + 0.5 \text{ M Na}_2\text{HCitr} + 0.4 \text{ M Na}_2\text{WO}_4 + 1.5 \text{ M NH}_3$  (where “Me” represents the iron group metal or total concentration of the iron group metal) at pH 7.5–8.5. The films of thickness

$10 \mu\text{m} - 12 \mu\text{m}$  are smooth and brilliant without any organic additives, and those electrodeposited at lower current densities are crack-free. Introduction of phosphorous into the alloys eliminates the cracks even at higher current densities. The electrodeposits are well-adhered to the Cu-substrate.

2. The amount of tungsten in Co-W alloys does not depend on current densities applied over a wide range and can reach 30 at.%. In the case of the Co-Ni-W alloys, the amount of tungsten decreases from 30 at.% to 14 at.% with increasing Ni(II) concentration in the bath and Ni in alloys. The deposit concentration of the ternary alloys is a balance between the induced and anomalous resulted co-deposition mechanism. The inclusion of P affected these mechanisms.

3. W-containing alloys (Co-W, and Co-Ni-P-W) co-deposited with phosphorous results in a significant decrease in the amount of tungsten especially at higher ratios of Ni(II) to Co(II) in the bath. This is the result of the comparatively easier P co-deposition with nickel than with cobalt and tungsten in the presence of nickel. There are no anomalous co-deposition Co with Ni in the presence of P noticed, i. e. the amount of Ni in the quaternary alloys linearly depends on the Ni(II) concentration in the alloys.

4. The baths having the same composition can be used both for film and nanostructures electrodeposition. In the latter case the electrodeposition under constant or pulse potential mode can be used to deposit nanotubes or nanowires, respectively.

#### Acknowledgments

The study was partially supported by INTAS foundation (INTAS Ref. Nr 15 – 104 – 7540). Moreover, partial support was provided by the US National Science Foundation CBET-#0231279. Also, H.C. thanks the Fulbright foundation for partial financial support of this study.

#### REFERENCES

1. Yao, S., Zhao, H., Kowaka, M. A New Amorphous Alloy Deposit with High Corrosion Resistance *Corrosion* 52 (3) 1996: pp. 183–186.
2. Abdel Hamid, Z. Electrodeposition of Cobalt–tungsten Alloys from Acidic Bath Containing Cationic Surfactants, *Materials Letters* 57 2003, pp. 2558–2564.
3. Kohn, A., Eizenberg, M., Shacham-Diamand, Y., Israel, B., Sverdlov, Y. Electroless Co(Mo,P) Films for Cu Interconnect Application *Microelectronic Engineering* 64 (1) 2002: pp. 315–320.
4. Atanasov, N., Gencheva, K., Bratoeva, M. Properties of Nickel-tungsten Alloys Electrodeposited from Sulfamate Electrolytes *Plating & Surface Finishing* 84 (2) 1997: pp. 67–71.
5. Ved, M., Sakhnenko, M., Nenastina, T., Bairachna, T., Korniy, S. Corrosion and Catalytic Properties of Galvanic Binary  $d^{6-8}$  Metal Alloys *Physicochemical Mechanics of Materials* 7 2008: pp. 346–353 (in Ukrainian).
6. Santana, R.A.C., Campos, A.R.N., Medeiros, E.A., Oliveira, A.L.M., Silva, L.M.F., Prasad, Sh. Studies on Electrodeposition and Corrosion Behavior of a Ni–W–Co Amorphous Alloy *Journal of Materials Science* 42 (22) 2007: pp. 9137–9144.
7. Romankiw, L. T. A Path: from Electroplating Through Lithographic Masks in Electronics to LIGA in MEMS *Electrochimica Acta* 42 (20–22) 1997: pp. 2985–3005.

8. **Lowe, H., Ehrfeld, W., Diebel, J.** Ultraprecision Microelectroforming of Metals and Alloys *Proceeding of SPIE* 3223 1997: pp. 168–175.
9. **Ehrfeld, W., Hessel, V., Lowe, H., Schulz, Ch., Weber, L.** Materials of LIGA Technology *Microsystem Technologies* 5 1999: pp. 105–112.
10. **Hubbart Jr., P. B., Podlaha, E. J.** The Study of Induced Codeposition of Ni-W Alloys, 1997<sup>th</sup> Meet.- Toronto (Canada). – May 14–18, 2001.
11. **Belevsky, S., Dikumar, A., Tsyntsar, N., Celis, J.-P.** Sliding and Wear-resistance of Electrodeposited Co-W Coatings: Dependence on Synthesis Parameters *Proc.Int. Conf. BALTRIB'2007* Kaunas, 21–23 Nov. 2007: pp. 111–116.
12. **Donten, M.** Bulk and Surface Composition, Amorphous Structure, and Thermocrystallization of Electrodeposited Alloys of Tungsten with Iron, Nickel and Cobalt *Journal of Solid State Electrochemistry* 3 1999: pp. 87–96.
13. **Cesiulis, H., Baltutiene, A., Donten, M., Donten, M. L., Stojek, Z.** Increase in Rate of Electrodeposition and in Ni(II) Concentration in the Bath as a Way to Control Grain Size of Amorphous / Nanocrystalline Ni-W Alloys *Journal of Solid State Electrochemistry* 6 2002: pp. 237–244.
14. **Vasauskas, V., Padgurskas, J., Rukuiža, R., Cesiulis, H., Celis, J.-P., Milčius, D., Prosyčev, I.** Cracking Behavior of Electrodeposited Nanocrystalline Tungsten-Cobalt and Tungsten-Iron Coatings *Mechanika (ISSN 1392-1207)* 4 2008” pp. 21–27.
15. **Donten, M., Stojek, Z., Cesiulis, H.** Formation of Nanofibres in Thin Layers of Amorphous W Alloys with Ni, Co and Fe Obtained by Electrodeposition *Journal of the Electrochemical Society* 150 (2) 2003: pp. C95–C98.
16. **Donten, M., Cesiulis, H., Stojek, Z.** Electrodeposition and Properties of Ni-W, Fe-W and Fe-Ni-W Amorphous Alloys. A Comparative Study *Electrochimica Acta* 45 (11) 2000: pp. 3389–3396.
17. **Kublanovsky, V., Bersirova, O., Dikumar, A., Bobanova, Zh., Cesiulis, H., Sinkeviciute, J., Prosyčev, I.** Electrodeposition and Corrosion Properties of Nanocrystalline Fe-W Alloys *Physicochemical Mechanics of Materials (ISSN 0430-6252)* 7 2008: pp. 308–314.
18. **Eliaz, N., Sridharand, T. M., Gileadi, E.** Synthesis and Characterization of Ni-W Alloys by Electrodeposition *Electrochimica Acta* 50 (14) 2005: pp. 2893–2904.
19. **Cesiulis, H., Podlaha-Murphy, E. J.** Electrolyte Considerations of Electrodeposited Ni-W Alloys for Microdevice Fabrication *Materials Science (Medžiagotyra)* 9 (4) 2003: pp.324–327.
20. **Azzaroni, P., Schilardi, L., Salvarezza, R. C.** Templated Electrodeposition of Patterned Soft Magnetic Films *Applied Physical Letters* 80 2002: pp. 1061–1063.
21. **Masuda, H., Yamada, Y., Satoh, M., Asoh, H., Nakao, M., Tamamura, T.** Highly Ordered Nanochannel-array Architecture in Anodic Alumina *Applied Physical Letters* 71 1997: pp. 2770–2777.
22. **Wang, J. B., Zhou, X. Z., Liu, Q. F., Xue, D. S., Li, F. S., Li, B., Kunkel, H. P., Williams, G.** Magnetic Texture in Iron Nanowire Arrays *Nanotechnology* 15 2004: pp. 485–489.
23. **Xue, D., Shi, H.** The Fabrication and Characteristic Properties of Amorphous Fe<sub>1-2x</sub>P<sub>x</sub> Alloy Nanowire Arrays *Nanotechnology* 15 2004: pp. 1752–1755.
24. **Xu, J., Huang, X., Xie, G., Fang, Y., Liu, D.** Fabrication and Magnetic Property of Monocrystalline Cobalt Nanowire Array by Direct Current Electrodeposition *Materials Letters* 59 2005: pp. 981–984.
25. **Qinv, D. H., Peng, Y., Cao, L., Liv, H. L.** A Study of Magnetic Properties: Fe<sub>x</sub>Co<sub>1-2x</sub> Alloy Nanowire Arrays *Chemical Physics Letters* 374 2003: pp. 661–666.
26. **Huang, Q., Davis, D., Podlaha, E. J.** Electrodeposition of FeCoNiCu Nanowires *Journal of Applied Electrochemistry* 36 (8) 2006: pp. 871–882.
27. **Davis, D. M., Moldovan, M., Young, D. P., Henk, M., Xie, X., Podlaha, E. J.** Magnetoresistance in Electrodeposited CoNiFe/Cu Multilayered Nanotubes *Electrochemical and Solid State Letters* 9 (9) 2006: pp. C153–C155.
28. **Huang, Q., Young, D. P., Chan, J. Y., Jiang, J., Podlaha, E. J.** Electrodeposition of FeCoNiCu/Cu Compositionally Modulated Multilayers *Journal of the Electrochemical Society* 149 (6) 2002: pp. C349–C354.
29. **Wen, S., Szpunar, J. A.** Direct Electrodeposition of Highly Ordered Magnetic Nickel Nanowires on Silicon Wafer *Micro & Nano Letters* 1 (2) 2006: pp. 89–93.
30. **Donten, M., Cesiulis, H., Stojek, Z.** Electrodeposition of Amorphous/Nanocrystalline and Crystalline Ni-Mo Alloys from Pyrophosphate Baths *Electrochimica Acta* 50 (6) 2005: pp. 1405–1412.
31. **Elsener, B., Atzei, D., Krolkowski, A., Rossi, A.** Effect of Phosphorus Concentration on the Electronic Structure of Nanocrystalline Electrodeposited Ni-P Alloys: an XPS and XAES Investigation *Surface and Interface Analysis* 40 (5) 2008: pp. 919–926.
32. **Ross, C. A.** Electrodeposited Multilayer Thin Films *Annual Review of Material Science* 24 1994: pp. 159–188.
33. **Grabco, D. Z., Dikumar, A. I., Petrenko, V. I., Harea, E. E., Shikimaka, O. A.** Micromechanical Proprieties of Co-W Alloys Electrodeposited Under Pulse Conditions *Elektronnaya Obrabotka Materialov (Surface Engineering and Applied Electrochemistry)* 1 2007: pp. 16–24.
34. **Donten, M., Stojek, Z., Osteryoung, J.G.** Voltammetric, Optical, and Spectroscopic Examination of Anodically Forced Passivation of Co-W Amorphous Alloys *Journal of the Electrochemical Society* 140 1993: p. 3417.
35. **Younes, O.; Zhu, L.; Rosenberg, Y; Shacham-Diamand, Y., Gileadi, E.** Electroplating of Amorphous Thin Films of Tungsten/Nickel Alloys *Langmuir* 17 (26) 2001: p. 8270-5.
36. **Silk, S. A., Tinkov, O. V., Petrenko, V. I., Tsyntsar, N. I., Dikumar, A. I.** Electrodeposition of Co-W Alloys: The Role of Temperature *Surface Engineering and Applied Electrochemistry* 4 2006: pp. 11–18 (in Russian).
37. **Podlaha, E. J., Landolt, D.** Induced Codeposition. III. Molybdenum Alloys with Nickel, Cobalt and Iron *Journal of the Electrochemical Society* 144 (5) 1997: pp.1672–1679.
38. **Ahmad, J., Asami, K., Takeuchi, A., Inoue, A.** Effect of Sodium Hypophosphite on the Structure and Properties of Electrodeposited Ni-W-P Alloys *Material Transactions* 44 (4) 2003: pp. 705–708.
39. **Sotskaya, N. V., Dolgikh, O. V.** Kinetics of Cathodic Reduction of Hypophosphite Anions in Aqueous Solutions *Russian Journal of Electrochemistry* 41 (12) 2005: pp. 1336–1340.
40. **Matlosz, M.** Competitive Adsorption Effects in the Electrodeposition of Iron-Nickel Alloys *Journal of the Electrochemical Society* 140 (8) 1993: pp. 2272–2279.
41. **Tarozaitė, R., Stalnionis, G., Sudavicius, A., Kurtinaitiene, M.** Change of Magnetic Properties of Autocatalytically Deposited CoNiP Films by Electrolysis Simultaneously Applied *Surface and Coatings Technology* 138 2001: pp. 61–70.